Electrical Sensing of Molecular Spin State Switching in a Spin Crossover Complex Using an Organic Field-Effect Transistor

Yuteng Zhang, Seyed Ehsan Alavi, Ion Soroceanu, Dennis Wanyoike Kamau, Aurelian Rotaru, Isabelle Séguy, L. Salmon, Gábor Molnár, Azzedine Bousseksou

ADVANCED ELECTRONIC MATERIALS Open Access
www.advelectronicmat.de

Electrical Sensing of Molecular Spin State Switching in a Spin Crossover Complex Using an Organic Field-Effect Transistor

Yuteng Zhang, Seyed Ehsan Alavi, Ion Soroceanu, Dennis Wanyoike Kamau, Aurelian Rotaru, Isabelle Séguy, Lionel Salmon, Gábor Molnár, and Azzedine Bousseksou**

An organic semiconductor – spin crossover polymer composite heterostructure is fabricated, and it is integrated into an organic field-effect transistor (OFET) with the aim to achieve electrical sensing of molecular spin state switching events. The OFETs display ≈50–70% increase in drain-source current intensity when going from the low spin (LS) to the high spin (HS) state. This phenomenon is reversible without apparent fatigue and the application of a gate voltage significantly enhances the sensing sensitivity. Capacitance measurements and finite element calculations allow identifying mechanical stress, induced by the spin state switching, at the origin of the transistor response. These results open up appealing perspectives for the integration of spin crossover molecules into technological applications, such as soft robotics .

1. Introduction

Molecular switches have received increasing attention as building blocks to store and manipulate information as well as to transduce different forms of energy.[1] Among the large variety of switchable molecules, spin-crossover (SCO) complexes of $3d^4$-$3d^7$ transition metal ions are renowned for their ability to switch reversibly between their low spin (LS) and high spin (HS) electronic configurations.[2—5] The switching between the two spin states can be triggered by various external stimuli such as temperature, pressure, light or X-ray irradiation, or by chemical substances. The SCO results in a significant alteration of the volume, magnetic, optical, caloric, mechanical and electronic properties of the material, thereby generating prospects for utilizing SCO molecules in different technological domains,[6,7] including memory devices,[8,9] active photonic devices,[10–12] temperature, pressure and gas sensors,[13–16] mechanical actuators,[17–19] heat management, and thermal energy harvesting systems.[20–23]

In many applications, such as in mechanical actuators or memory devices, it appears vital to have the capability to induce as well as to detect the spin state changes using integrated electrical circuits. Switching can be relatively easily implemented by electrothermal means, e.g. by intoducing a Joule-heated element into the system.[24] On the other hand, direct electrical sensing is usually not possible because the changes of capacitance and/or conductance accompanying the SCO phenomenon are relatively weak and remain difficult to detect in situ.[25,26] To address this important issue, several approaches have been proposed. E.g., chemists synthesized sophisticated SCO complexes incorporating conducting molecular bricks, such as $TCNQ^{n-}$ (7,7′,8,8′-tetracyanoquinodimethane). However, the effective synergy between the charge transport and SCO phenomena could be demonstrated only in a few cases.[27,28] A similar, but more versatile approach uses a mixture of the SCO material with electroactive polymers (e.g., polypyrrole or poly(vinylidene fluoride-co-trifluoro-ethylene)), the resulting composites showing easily measurable resistance switching[29,30] or current discharge[23] at

Y. Zhang, S. E. Alavi, L. Salmon, G. Molnár, A. Bousseksou
LCC
CNRS
University of Toulouse
UPS
INP
Toulouse F-31077, France
E-mail: gabor.molnar@lcc-toulouse.fr;
azzedine.bousseksou@lcc-toulouse.fr
Y. Zhang, D. W. Kamau, I. Séguy
LAAS
CNRS, University of Toulouse
INSA
UPS
Toulouse F-31077, France
I. Soroceanu, A. Rotaru
Faculty of Electrical Engineering and Computer Science and MANSiD Research Center
Stefan cel Mare University
13, Strada Universitatii, Suceava 720229, Romania

The ORCID identification number(s) for the author(s) of this article can be found under https://doi.org/10.1002/aelm.202400590

DOI: 10.1002/aelm.202400590

the SCO. The underlying general idea is to use the volume expansion/contraction of the molecules accompanying the change of spin state to modulate the electrical properties of the polymers via electromechanical coupling (i.e., via piezoresistive or piezoelectric effects). Alternatively, besides polymers, inorganic conducting compounds (e.g., metallic nanoparticles) were also successfully used to obtain conducting hybrid SCO materials.[31,32]

From a practical point of view, however, it is sometimes preferable to avoid mixing materials and process them instead in a multilayer device structure. At the macroscopic scale, this idea was first demonstrated using a bilayer cantilever structure combining two polymer composite films, one being piezoresistive and another SCO-active, generating a sharp resistance change at the SCO due to the bending of the cantilever.[33] More micro/nanotechnology-oriented approaches aimed at modulating current injection into nanoscale SCO junctions[34–36] or coupling SCO films to ferroelectric substrates[9] or integrating SCO films into microelectomechanical systems (MEMS).[18] Another effective strategy combines atomically flat, 2D materials (mostly graphene) with SCO compounds. The first device of this type was reported in 2017 wherein $[Fe(Htrz)_2(trz)]BF_4$ (Htrz = 1H-1,2,4-triazole, trz- = deprotonated triazolato ligand) nanoparticles were deposited onto a graphene layer, embedded in a three-terminal device, giving rise to a reversible change (≈25%) in the conductance of graphene upon the SCO.[37] Subsequently, several other graphene-based devices incorporating different SCO materials were reported, including SCO single crystals,[38,39] nanoparticles[40,41] and evaporated films,[42,43] the two materials being either in direct contact or separated by a spacer. In most cases, the resistance changes remained relatively modest (a few percent), but well detectable. As for the mechanism, which couples the SCO to the conduction of graphene, several hypothesis have been evoked, including mechanical strain[39] and electrostatic effects,[38,41] but at present this question remains open to discussion.

In the present paper, we explore a novel strategy for electrical sensing of spin state switching, based on strain coupling between a pressure sensitive organic semiconductor (OSC) layer and a polymer:SCO composite layer, integrated in an OFET architecture. The expectation is that the volume strain associated with the thermally-induced SCO event should give rise to mechanical stress in the OSC layer. Due to the high compressibility of the latter, the distance between the conductive backbones will be then altered, directly modifying thus the charge transport in the OFET channel. Whereas one could use more simple two-terminal device configurations, there are several advantages in employing OFETs for sensing applications.[44–46] First, OFETs combine sensing and switching functions, providing both high sensitivity as well as high integration density and including even the possibility to create sensing matrices. By the same token, they afford also for various potentially useful detection signals (e.g., drain– source current, threshold voltage, current switching ratio). In addition, OFETs can be fabricated on flexible substrates, they are lightweight and can be deployed thus advantageously in wearable and embarked systems. Here, we show that OFETs can be used to detect changes of molecular spin states and demonstrate a well reproducible (>30 switching events) increase of the drain-source current intensity by typically 50 –70% when going from the LS to the HS state. Using finite element analysis (FEA), we trace back the changes in current intensity to the mechanical stress generated by the SCO molecules in the OSC layer and provide guidelines for further optimization of the mechanical coupling.

2. Results and Discussion

The schematic cross-section of our bottom-gate, bottom-contact OFET device, with a polymer:SCO composite film deposited on top of the OSC layer, is shown in **Figure 1a**. The main fabrication steps of the device can be depicted in Figure 1b. Heavily doped n-type ($\rho \approx 10^{-3}$ Ω.m) silicon substrates were used with a 225 nm thick SiO_2 top layer, which serves as gate dielectric. Source (S), drain (D), and gate (G) electrodes (Cr/Au) were patterned by photolithography, forming a channel with a width of W = 1000 µm and a length of L = 70 µm (except otherwise mentioned). After surface treatment, the substrates were transferred into a glove box for the remaining fabrication steps, which include spin coating and patterning of a 100 nm thick OSC layer, followed by spin coating of a 450 nm thick polymer:SCO layer and, finally, the encapsulation of the active area using a glass slide and epoxy sealing. The thicknesses of the OSC and polymer:SCO layers were confirmed by scanning electron microscopy (SEM) and atomic force microscopy (AFM) imaging (see Figure 1c,d).

Among the various reported OSC materials, we have selected for our work the widely used polymer, poly(3-hexylthiophene) (P3HT), for two main reasons: its known sensitivity to mechanical strain,[47,48] combined with a robust and linear temperature-dependent mobility up to ≈100–120 °C.[49,50] The latter criterion is particularly important as we use in our experiments the "benchmark" SCO complex $[Fe(Htrz)_2(trz)]BF_4$, which presents one of the largest volume change upon the SCO (≈10%), but must be heated to relatively high temperatures to reach the fully populated HS state. (N.B. At this point, it is worth to note that in contrast to the compound $[Fe(Htrz)_2(trz)]BF_4$, most technologically relevant SCO compounds display spin transition closer to room temperature, i.e., <70 °C.[8,12,13,15,19]) Although the presence of a polymer matrix is not mandatory, we decided to embed SCO particles in a polymer because this is the most general way how SCO materials are processed for practical applications.[51] The choice of the polymer matrix is dictated by four important factors: (i) its insulating nature, (ii) the orthogonality of its solvent with respect to both the SCO particles and the P3HT layer, (iii) its relatively high elastic modulus and (iv) its thermal stability. Of particular importance is to avoid polymers with a glass transition near the SCO temperature range. Taking into account these criteria, we opted for PVP (polyvinylpyrrolidone) dissolved in ethanol, which is a poor solvent for P3HT.[52] PVP was mixed with 50 wt% SCO nanoparticles made of silica-coated $[Fe(Htrz)_2(trz)]BF_4$, which is a benchmark in the field.[53] At this point, it should be noted that there are potentially several ways to introduce SCO molecules into an OFET structure. E.g., they can be deposited at the interface between the gate dielectric and OSC layer or mixed with the OSC layer or even mixed with the gate dielectric (if it is made of a polymer). However, all these approaches can strongly degrade the transistor output and transfer characteristics. This is why we opted for depositing the SCO composite as the uppermost layer, "far away" from the very sensitive conducting

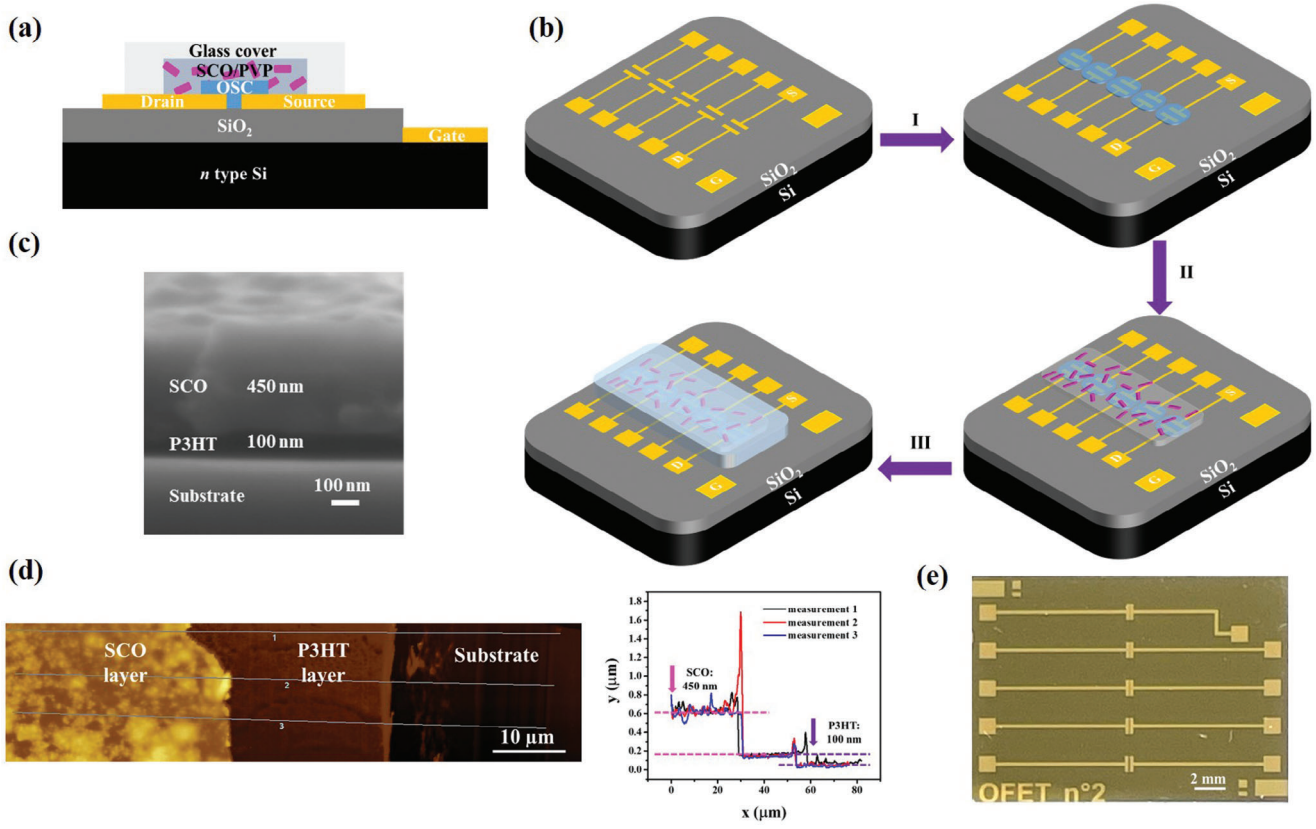

Figure 1. Schemes of a) the cross-section and b) the fabrication process of the PVP:SCO/OFET device: I. P3HT deposition and patterning, II. PVP:SCO deposition, and III. device encapsulation. c) SEM image of the device cross-section. d) AFM topography image and cross-sections showing the three layers near a scratch in the films and e) photograph of a chip with the patterned electrodes.

channel, which is located in a few nm thick layer of the OSC film at the interface with the dielectric (see Figure S1a, Supporting Information).[54]

Figure 2a shows the room temperature output characteristics of a "reference" OFET device, prepared without PVP top layer. The output curves show a characteristic saturation in drain-source current (I_{DS}) as the drain-source voltage (V_{DS}) increases negatively at a fixed gate voltage (V_G), typical for a p-type OFET device. When this device is coated with a pure PVP film (i.e., without SCO particles), we obtained fairly similar characteristics (Figure 2b), confirming thus that the PVP deposition does not strongly modify the transistor performance, even if it remains a limiting step in terms of device reproducibility. One shall note the relatively low I_{ON}/I_{OFF} ratio of our devices (≈1 – 2 decades), which is possibly linked to leakage currents.[55] It should be, however, underlined that a trade-off was necessary between the output characteristics and the thermal behavior of the devices. In fact, using slightly different fabrication protocols, we were able to fabricate devices with substantially higher ON/OFF ratios (see Figure S1, Supporting Information).

However, for the present work, linear and reversible behavior upon thermal cycling is also a key asset. This is why we opted for a fabrication protocol affording for poorer output characteristics, but more suitable thermal behavior. This important asset can be clearly depicted in Figure 2 (right panels), which shows the variation of I_{DS} upon three successive thermal cycles between 40 and 120 °C. Apart from the well-known first "run-in cycle", which occurs inevitably during the first heating due to the loss of residual solvents and microstructural changes,[13] the current intensity shows indeed a fairly reproducible, linear increase/decrease upon heating/cooling due to thermally activated processes. Taking into account literature reports on the delicate interplay between temperature treatments, crystalline structure, grain/interfacial morphology and charge transport in P3HT,[50,56,57] there is clearly still room for improving the output characteristics, thermal stability and reproducibility of our devices. Nevertheless, the present configuration is fully suitable for proof-of-concept studies with integrated SCO materials.

As shown in **Figure 3a**, the room temperature output characteristics of the PVP:SCO/OFET device, integrating SCO particles, are comparable with that of the "reference" device. On the other hand, the temperature dependent characteristics turned out to be drastically different due to the SCO phenomenon. Figure 3b (see also Figure S2, Supporting Information) displays the variation of I_{DS} upon three successive thermal cycles between 40 and 120 °C in the ON state of the transistor (V_G = −10 V, V_{DS} = −30 V). One can clearly depict an abrupt increase of the current intensity near 100 °C on heating and the reverse phenomenon near 65 °C on cooling, denoting a thermal hysteresis loop of ≈35 °C width, well known for the SCO compound $[Fe(Htrz)_2(trz)]BF_4$.[53]

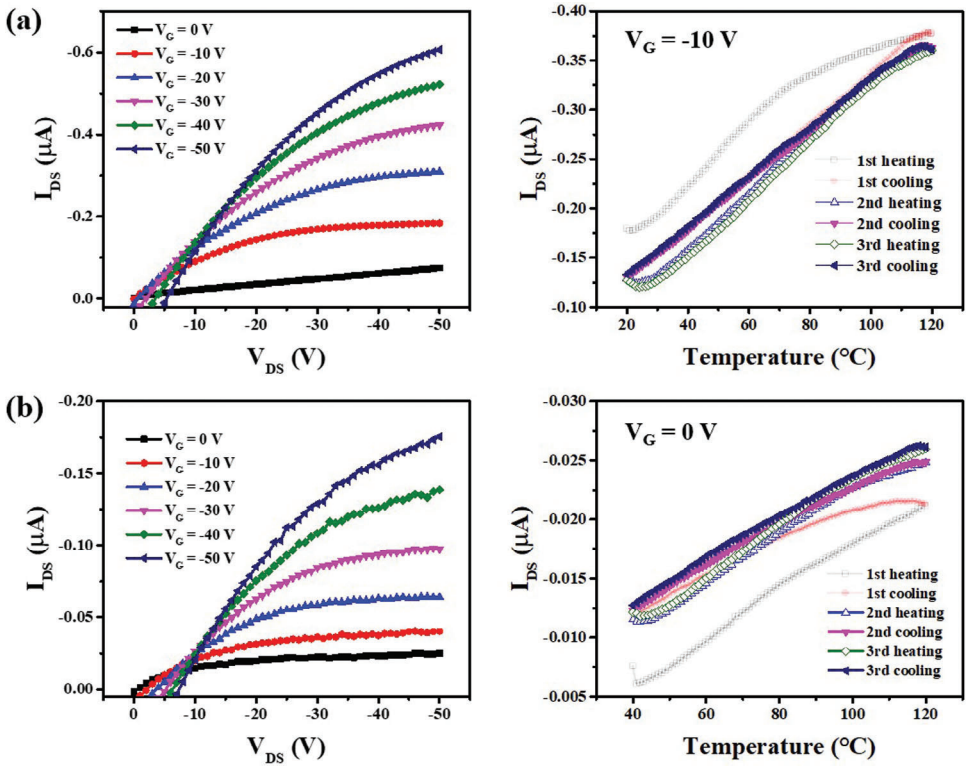

Figure 2. Characterization of "reference" OFET (a) and PVP/OFET (b) devices without SCO particles. Left panels: Output characteristics at room temperature. Right panels: drain-source current during three successive thermal cycles (V_{DS} = −30 V, dT/dt = ± 2 °C/min).

Indeed, a comparison with the optical absorbance changes of the PVP:SCO/P3HT bilayer in Figure 3b confirms obviously that the origin of this hysteresis is the SCO phenomenon. This hysteresis is particularly useful to distinguish the effect of SCO from any other possible thermal effects on the charge mobility. Indeed, at a fixed temperature inside the hysteresis loop (e.g., 80 °C), we observe a ≈60% more intense drain-source current in the HS state when compared to the LS form. As mentioned before, in the ON state of the transistor, the conduction channel is restricted to the first few nm near the interface with the gate dielectric.[54] In other words, the conduction channel and the SCO composite film are separated by a ≈95 nm thick P3HT layer wherein the charge transport is negligible. In this respect, the spin transition effects observed on the device can be considered "contactless". Interestingly, even if we set the gate voltage to 0 V, the current switching between the LS and HS states is still observable (via the leakage current) with roughly the same relative change (see Figure 3c). Nevertheless, the comparison between Figure 3b,c denotes clearly the interest of using a gate voltage in terms of sensing sensitivity. (N.B. One should note here that the gate voltage is not expected to alter the spin state of the SCO compound because the electrical field in the SCO layer is negligible in our device configuration and, in any case, the spin state of SCO complexes is not significantly sensitive to an applied field).[23]

Importantly, the SCO-induced switching of transistor output could be perfectly reproduced in several devices–fabricated with different channel lengths (ranging from 10 to 110 μm), both in the linear and saturation regimes (see Figure S4, Supporting Information). Besides, to confirm the good reversibility and lack of significant fatigue effects, on one of these devices we performed multiple thermal cycles (overall 30 switching events), which are shown in Figures 3d and S3, Supporting Information.

The starting hypothesis of our work was the idea of establishing mechanical coupling between the spin state change in the SCO film and the charge transport in the OSC layer. However, the SCO phenomenon involves substantial changes of the polarizability and dipole moment of the complexes, which may also impact the charge transport in the organic semiconductor layer due to the modification of the electrostatic potential. Based on a computational approach, van Geest et al.[38] argued that this phenomenon should be at the origin of the conductivity switching in their graphene-based transistor. However, contrary to their work, which used a single, oriented SCO crystal, in the present case the SCO material consists of more or less randomly oriented particles within the polymer matrix. In this situation, one shall not expect a considerable variation of the electrostatic potential near the PVP:SCO layer. It may be worth to note also that in our experimental situation the electrical field within the PVP:SCO layer is weak. Nevertheless, to bring more light into this question, we carried out capacitance measurements on the PVP:SCO film in the two spin states at identical temperatures (in the middle of the hysteresis loop), in a broad frequency range. As shown in **Figure** 4a,b, we could observe only minor capacitance changes (less than 2%) when going from the LS to the HS state, which cannot rationalize an electrostatic mechanism.

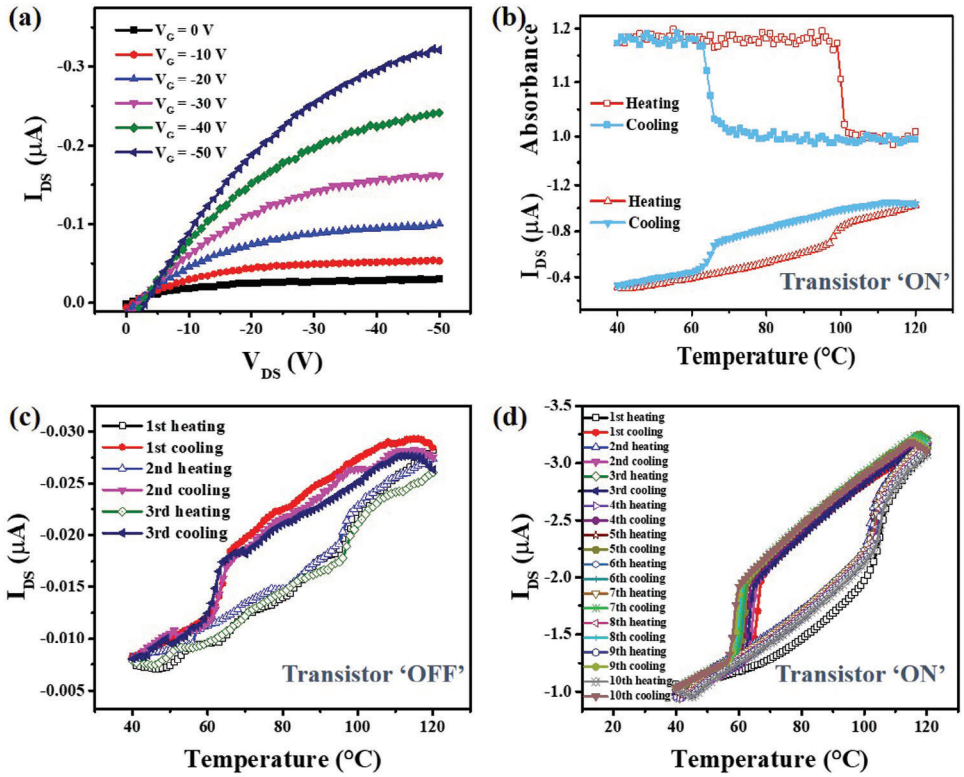

Figure 3. Characterization of the PVP:SCO/OFET devices. a) Output characteristics at room temperature. b,c) Drain-source current during three successive thermal cycles recorded for $V_{DS} = -30$ V, dT/dt = ± 2 °C/min and b) $V_G = -10$ V, or c) $V_G = 0$ V. For comparison, the UV absorbance change (at 350 nm) of the PVP:SCO/P3HT bilayer film is also shown in (b). d) Drain-source current during ten successive thermal cycles for a second device with different channel length (L = 30 μm) recorded for $V_G = -10$ V, $V_{DS} = -30$ V, dT/dt = ± 2 °C/min.

A more plausible explanation is related to the known sensitivity of P3HT to mechanical stress and strain.[47,48] In general, charge transport in organic semiconductors can be significantly modulated under an applied load due to their relatively high compressibility.[58,59] Gao et al.[48] has investigated the piezoresistance of P3HT under uniaxial compressive load in a two-terminal configuration and found a considerable increase of the current intensity (by a factor of 2–10). The authors suggested that changes in the polymer microstructure, such as the decrease in the distance between the neighboring conductive backbones, could be responsible for the conductivity improvement. To analyze the mechanical stress and strain generated in the P3HT layer due to the SCO phenomenon in our PVP:SCO/OFET devices, we have carried out a series of finite element simulations using the commercial ABAQUS software. The calculation details, geometries and thermomechanical properties of the simulated structures are given in Supporting Information. For the lack of accurately determined thermomechanical properties, these computations provide only indications of the sign and magnitude of changes in stress and strain when going through the spin transition. Of particular interest for us is the variation of the in-plane stress (σ_{11}) in the P3HT conducting channel (i.e., in the

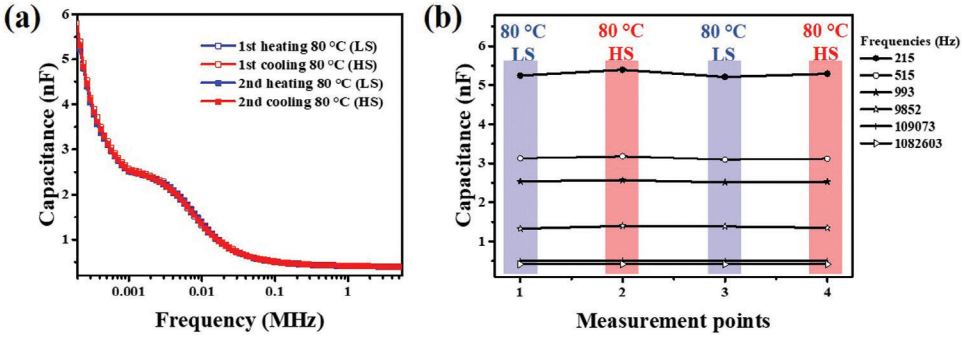

Figure 4. a) Capacitance of a PVP:SCO film as a function of the frequency of the applied electrical field, recorded at 80 °C through two heating-cooling cycles. b) Capacitance recorded at selected frequencies at 80 °C, either on heating (LS state – blue) or on cooling (HS state – red).

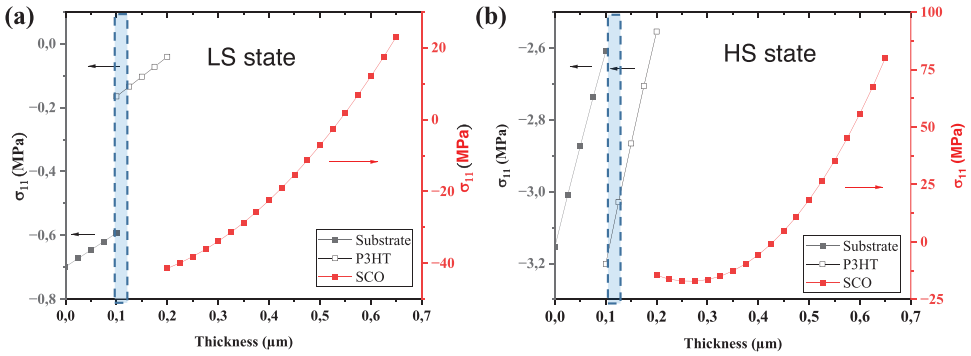

Figure 5. FEA simulations of the in-plane stress component σ_{11} through the thickness of the stack, halfway between the source and drain electrodes, in the LS (a) and HS (b) states. The blue shaded area indicates roughly the position of the conducting channel in the P3HT layer.

proximity of the interface with the SiO_2 substrate). The contour plots of σ_{11} in the two spin states are shown in Figure S7 (Supporting information), visually revealing the change of stress distribution within the OFET structure upon the SCO. In a more quantitative manner, the computed values of stresses before and after the spin transition are plotted in **Figure 5** for the in-plane, and in Figure S8 (Supporting Information), for the out-of-plane directions, respectively. Note that these figures show the stress along the thickness of the multilayer structure, halfway between the source and drain electrodes.

As shown in Figure 5a, before the spin transition (LS state) a weak mechanical stress (≈−0.15 MPa) arises within the conduction channel due to the thermal expansion mismatch of the different layers. The intrinsic mechanism caused by the thermally induced switching of the spin state of the particles is an expansion of metal-ligand bond lengths in the SCO complex, which results in a volume expansion of the entire PVP:SCO composite. Since the composite film is mechanically clamped to the substrate, the in-plane expansion transforms into an in-plane stress both in the PVP:SCO and P3HT layers (Figure 5b), altering thus the charge transport in the latter. Specifically, within the conduction channel of the OFET the compressive stress increases to ≈−3.2 MPa due to the SCO phenomenon. We can link this SCO-induced mechanical stress in the P3HT to its electrical resistance by considering the above-mentioned experimental observations of Gao et al.[48] on the piezoresistive properties of P3HT. According to these authors, compressive stresses of the order of a few hundreds of kPa result in a sizable increase of the charge mobility, which is in agreement with our experimental observation of a sudden increase of the drain-source current when going from the LS to the HS state. It is important to underline that the stress generated by the SCO phenomenon within the OSC layer strongly depends on the elastic moduli of the materials. In the present case, the PVP matrix has a fairly high modulus (≈2 GPa), which affords for generating relatively high stress levels within the structure due to the SCO.[58] On the other hand, the elastic modulus of P3HT is relatively low (≈120 MPa), but in this case the high piezoresistive coefficient remains the most important figure of merit. We anticipate that this type of FEA simulations should increasingly serve in the field to analyze and predict the effects of different design parameters (mechanical properties, geometry, etc.).

3. Conclusions

In summary, we fabricated PVP:SCO/P3HT hybrid OFET devices capable of electrically sensing molecular spin state changes in thin polymer composite films at the micrometer scale. The drain-source current in the device increased reversibly by 50–70% when going from the LS to the HS state, which we attributed to compressive stresses generated in the P3HT layer due to the SCO. The use of an orthogonal solvent allowed for the liquid phase deposition of the PVP:SCO layer on top of the P3HT without much altering the transistor performance. We expect that this versatile method should enable the fabrication of devices with various combinations of SCO particles, polymer matrices, and organic semiconductor materials, providing potentially even higher strain sensitivity and lower spin transition temperatures. Interestingly, spin state sensing could be demonstrated even at zero gate voltage, but the switching ability of the three-terminal device appears as an important asset for future work as it affords both high sensitivity and high integration density. As such, these results broaden the realm for further integration of SCO materials into technological applications. In particular, we anticipate the development of lightweight, flexible devices[44,59,60] combining the mechanical actuation capability of polymer:SCO composites[18,19] with the strain sensitivity of organic electronic materials[61,62] providing scope for applications in soft robotics and related areas. On the other way around, one may also consider using SCO molecules for active tuning of OFET characteristics in a similar manner as it has been proposed using photochromic molecules.[63,64] The main interest in this "SCO for OFET" approach comes from the rich stimuli-responsive behavior of SCO molecules, which could significantly extend the sensing capability of OFET based sensor devices.

4. Experimental Section

Device Fabrication: For bottom gate, bottom contact OFET fabrication, pre-patterned substrates with source and drain electrodes were prepared on top of SiO_2 by Cr/Au (10 nm and 50 nm respectively) lift-off using 5 μm negative NLOF 2035 resist (purchased from MicroChemicals). The pre-patterned substrates were rinsed successively with acetone (VLSI, 99.5%) and ethanol (VLSI, 99.9%) for 5 min under sonication. They were then dried by a nitrogen gas flow, and cleaned by an oxygen plasma treatment (60 W, 2 min). The rest of the procedure was carried out in a glove box (O_2/H_2O < 3 ppm). For OSC deposition,

P3HT (regioregular, average M_n 54000 – 75000 g mol^{-1}; >98% head-to-tail, purchased from Sigma-Aldrich) was dissolved in chlorobenzene (15 mg mL^{-1}) and the solution was held on a hot plate (60 °C) under magnetic stirring for 4 h. This solution was then spin-coated onto the substrates at 1200 rpm for 30 s followed by a short annealing (120 °C, 1 min) in order to remove the residual solvent. The obtained P3HT film was then manually patterned to a smaller area. For the SCO deposition, the SCO NPs (synthesized as described earlier[65]) and PVP (40-50G, purchased from Sigma-Aldrich) were mixed with ethanol at concentrations of 50 mg mL^{-1} and spin-coated on top of the P3HT layer at 1200 rpm for 30 s, followed by a short annealing (80 °C, 1 min). Finally, for the device encapsulation, a glass slide was placed on the sample and sealed all around with a UV-curable epoxy (DELO Katiobond LP655).

Device Characterization: The SCO phenomenon in the films was detected by measuring the temperature dependent optical absorption spectrum using a Cary 50 (Agilent) spectrophotometer and a THMS600 (Linkam Scientific) heating-cooling stage. AFM surface topography images were acquired under ambient conditions in tapping mode using a SMART-SPM (Horiba) equipped with HQ:NSC15/Al BS probes (MikroMasch, 40 N m^{-1}, 300 kHz). SEM images were acquired in secondary electron mode using a Hitachi S4800 instrument. For the electrical characterization of the devices, a Keithley 6430 source-meter (V_{DS} and I_{DS}) together with a Keihley series 2400 voltage source (V_G) and a HFS350EV-PB4 (Linkam Scientific) heating-cooling stage equipped with three tungsten probes, was used. For capacitance measurements, 100 nm Al was thermally evaporated on the top of the PVP:SCO layer to form an Au/SCO/Al parallel plate capacitor, analyzed by an Agilent 4294A precision impedance meter (test signal amplitude: 10 mV, DC bias: 0 V) in conjunction with the HFS350EV-PB4 heating-cooling stage.

Supporting Information

Supporting Information is available from the Wiley Online Library or from the author.

Acknowledgements

This project has received funding from the European Research Council (ERC) under the European Union's Horizon 2020 research and innovation program (Grant Agreement No. 101019522) and from the French government, through the France 2030 project managed by the National Research Agency (ANR) with the reference number "ANR-22-EXES-0015". Technical realizations were partly supported by the French RENATECH network. The authors thank Y. Zan and A. Enriquez-Cabrera (LCC-CNRS) for their support of SCO NPs synthesis, A. Laborde and L. Salvagnac (LAAS-CNRS) for their technical support in device preparation, and N. Mauran (LAAS-CNRS) for his technical support of electrical property characterization.

Conflict of Interest

The authors declare no conflict of interest.

Data Availability Statement

The data that support the findings of this study are available from the corresponding author upon reasonable request.

Keywords

mechanical strain, organic semiconductor, spin crossover, transistor

Received: July 24, 2024
Revised: August 23, 2024
Published online:

[1] *Molecular Switches* (Eds.: B. L. Feringa, W. R. Browne), Wiley-VCH-GmbH, Weinheim, Germany **2001**.
[2] P. Gütlich, A. Hauser, H. Spiering, *Angew. Chem., Int. Ed. Engl.* **1994**, *33*, 2024.
[3] *Spin-Crossover Materials: Properties and Applications* (Ed.: M. A. Halcrow), John Wiley & Sons, Chichester, UK **2013**.
[4] *Spin Crossover in Transition Metal Compounds I.-III., Topics in Current Chemistry*, vol. *233-235* (Eds.P. Gütlich, H. Goodwin), Springer, Berlin, Heidelberg, Germany, **2004**, 233.
[5] A. Bousseksou, G. Molnár, L. Salmon, W. Nicolazzi, *Chem. Soc. Rev.* **2011**, *40*, 3313.
[6] K. S. Kumar, M. Ruben, *Coord. Chem. Rev.* **2017**, *346*, 176.
[7] G. Molnár, S. Rat, L. Salmon, W. Nicolazzi, A. Bousseksou, *Adv. Mater.* **2018**, *30*, 1703862.
[8] O. Kahn, C. J. Martinez, *Science* **1998**, *279*, 44.
[9] G. Hao, A. Mosey, X. Jiang, A. J. Yost, K. R. Sapkota, G. T. Wang, X. Zhang, J. Zhang, A. T. N'Diaye, R. Cheng, X. Xu, P. A. Dowben, *Appl. Phys. Lett.* **2019**, *114*, 032901.
[10] O. Kahn, J. Kröber, J. C. Jay, *Adv. Mater.* **1992**, *4*, 718.
[11] P. Mounaix, E. Freysz, J. Degert, N. Daro, J. F. Létard, P. Kužel, V. Vigneras, L. Oyenhart, *Appl. Phys. Lett.* **2006**, *89*, 174105.
[12] K. Abdul-Kader, M. Lopes, C. Bartual-Murgui, O. Kraieva, E. M. Hernández, L. Salmon, W. Nicolazzi, F. carcenac, C. Thibault, G. Molnar, A. Bousseksou, *Nanoscale* **2013**, *5*, 5288.
[13] K. Ridier, A. C. Bas, Y. Zhang, L. Routaboul, L. Salmon, G. Molnár, C. Beragud, A. Bousseksou, *Nat. Commun.* **2020**, *11*, 3611.
[14] J. Linares, E. Codjovi, Y. Garcia, *Sensors* **2012**, *12*, 4479.
[15] M. Ohba, K. Yoneda, G. Agustí, M. C. Munoz, A. B. Gaspar, J. A. Real, J. A., J. A. Real, M. Yamasaki, H. Ando, Y. Nakao, S. Sakaki, S. Kitagawa, *Angew. Chem., Int. Ed.* **2009**, *48*, 4767.
[16] D. Gentili, N. Demitri, B. Schäfer, F. Liscio, I. Bergenti, G. Ruani, M. Ruben, M. Cavallini, *J. Mater. Chem. C* **2015**, *3*, 7836.
[17] H. J. Shepherd, I. A. Gural'skiy, C. M. Quintero, S. Tricard, L. Salmon, G. Molnár, A. Bousseksou, *Nat. Commun.* **2013**, *4*, 2607.
[18] M. D. Manrique-Juárez, F. Mathieu, A. Laborde, S. Rat, V. Shalabaeva, P. Demont, O. Thomas, L. Salmon, T. Leichle, L. Nicu, G. Molnár, A. Bousseksou, *Adv. Funct. Mater.* **2018**, *28*, 1801970.
[19] M. Piedrahita-Bello, J. E. Angulo-Cervera, A. Enriquez-Cabrera, G. Molnár, B. Tondu, L. Salmon, A. Bousseksou, *Mater. Horiz.* **2021**, *8*, 3055.
[20] S. P. Vallone, A. N. Tantillo, A. M. Dos Santos, J. J. Molaison, R. Kulmaczewski, A. Chapoy, P. Ahmadi, M. A. Halcrow, K. G. Sandeman, *Adv. Mater.* **2019**, *31*, 1807334.
[21] K. Ridier, Y. Zhang, M. Piedrahita-Bello, C. M. Quintero, L. Salmon, G. Molnár, C. Bergaud, A. Bousseksou, *Adv. Mater.* **2020**, *32*, 2000987.
[22] E. Resines-Urien, M. A. G. García-Tuñón, M. García-Hernández, J. A. Rodríguez-Velamazán, A. Espinosa, J. S. Costa, *Adv. Sci.* **2022**, *9*, 2202253.
[23] S. Rat, M. Piedrahita-Bello, L. Salmon, G. Molnar, P. Demont, A. Bousseksou, *Adv. Mater.* **2018**, *30*, 1705275.
[24] I. A. Gural'skiy, C. M. Quintero, J. S. Costa, P. Demont, G. Molnár, L. Salmon, H. J. Shepherd, A. Bousseksou, *J. Mater. Chem. C* **2014**, *2*, 2949.
[25] A. Bousseksou, G. Molnár, P. Demont, J. Menegotto, *J. Mater. Chem.* **2003**, *13*, 2069.
[26] A. Rotaru, I. A. Gural'skiy, G. Molnar, L. Salmon, P. Demont, A. Bousseksou, *Chem. Commun.* **2012**, *48*, 4163.
[27] M. Wang, Z. Y. Li, R. Ishikawa, M. Yamashita, *Coord. Chem. Rev.* **2021**, *435*, 213819.
[28] M. Nihei, N. Takahashi, H. Nishikawa, H. Oshio, *Dalton Trans.* **2011**, *40*, 2154.
[29] Y. S. Koo, J. R. Galán-Mascarós, *Adv. Mater.* **2014**, *26*, 6785.

[30] D. Nieto-Castro, F. A. Garcés-Pineda, A. Moneo-Corcuera, I. Sánchez-Molina, J. R. Galán-Mascarós, *Adv. Funct. Mater.* **2021**, *31*, 2102469.
[31] R. Torres-Cavanillas, M. Morant-Giner, G. Escorcia-Ariza, J. Dugay, J. Canet-Ferrer, S. Tatay, S. Cardona-Serra, M. Giménez-Marqués, M. Galbiati, A. Forment-Aliaga, E. Coronado, *Nat. Chem.* **2021**, *13*, 1101.
[32] R. Torres-Cavanillas, R. Sanchis-Gual, J. Dugay, M. Coronado-Puchau, M. Giménez-Marqués, E. Coronado, *Adv. Mater.* **2019**, *31*, 1900039.
[33] Y. C. Chen, Y. Meng, Z. P. Ni, M. L. Tong, *J. Mater. Chem. C* **2015**, *3*, 945.
[34] C. Lefter, S. Rat, J. S. Costa, M. D. Manrique-Juárez, C. M. Quintero, L. Salmon, I. Séguy, T. Leichle, L. Nicu, P. Demont, A. Rotaru, G. Molnár, A. Bousseksou, *Adv. Mater.* **2016**, *28*, 7508.
[35] V. Shalabaeva, K. Ridier, S. Rat, M. D. Manrique-Juarez, L. Salmon, I. Séguy, A. Rotaru, G. Molnar, A. Bousseksou, *Appl. Phys. Lett.* **2018**, *112*, 013301.
[36] L. Poggini, M. Gonidec, J. H. González-Estefan, G. Pecastaings, B. Gobaut, P. Rosa, *Adv. El. Mater.* **2018**, *4*, 1800204.
[37] J. Dugay, M. Aarts, M. Giménez-Marqués, T. Kozlova, H. W. Zandbergen, E. Coronado, H. S. J. Van Der Zant, *Nano Lett.* **2017**, *17*, 186.
[38] E. P. van Geest, K. Shakouri, W. Fu, V. Robert, V. Tudor, S. Bonnet, G. F. Schneider, *Adv. Mater.* **2020**, *32*, 1903575.
[39] C. Boix-Constant, V. García-López, E. Navarro-Moratalla, M. Clemente-León, J. L. Zafra, J. Casado, F. Guinea, S. Mañas-Valero, E. Coronado, *Adv. Mater.* **2022**, *34*, 2110027.
[40] J. F. Dayen, N. Konstantinov, M. Palluel, N. Daro, B. Kundys, M. Soliman, G. Chastanet, B. Doudin, *Mater. Horiz.* **2021**, *8*, 2310.
[41] K. Maity, J. F. Dayen, M. Palluel, N. Daro, G. Chastanet, B. Kundys, B. Doudin, *Appl. Phys. Lett.* **2023**, *123*, 163503.
[42] N. Konstantinov, A. Tauzin, U. N. Noumbé, D. Dragoe, B. Kundys, H. Majjad, A. Brosseau, M. Lenertz, A. Singh, S. Berciaud, M. L. Boillot, B. Doudin, T. Mallah, J. F. Dayen, *J. Mater. Chem. C* **2021**, *9*, 2712.
[43] M. Gavara-Edo, R. Córdoba, F. J. Valverde-Muñoz, J. Herrero-Martín, J. A. Real, E. Coronado, *Adv. Mater.* **2022**, *34*, 2202551.
[44] S. Yuvaraja, A. Nawaz, Q. Liu, D. Dubal, S. G. Surya, K. N. Salama, P. Sonar, *Chem. Soc. Rev.* **2020**, *49*, 3423.
[45] H. Sirringhaus, *Adv. Mater.* **2014**, *26*, 1319.
[46] P. Lin, F. Yan, *Adv. Mater.* **2012**, *24*, 34.
[47] P. Cosseddu, S. Milita, A. Bonfiglio, *IEEE Electron Device Lett.* **2012**, *33*, 113.
[48] L. Gao, Y. M. Tian, W. Hou, W. Q. Yan, G. Y. Zhong, *Adv. Polym. Technol.* **2018**, *37*, 21707.
[49] M. Song, J. Seo, H. Kim, Y. Kim, *ACS Omega* **2017**, *2*, 4065.
[50] S. Joshi, P. Pingel, S. Grigorian, T. Panzner, U. Pietsch, D. Neher, M. Forster, U. Scherf, *Macromolecules* **2009**, *42*, 4651.
[51] A. Enriquez-Cabrera, A. Rapakousiou, M. P. Bello, G. Molnár, L. Salmon, A. Bousseksou, *Coord. Chem. Rev.* **2020**, *419*, 213396.
[52] M. Roesing, J. Howell, D. Boucher, *J. Polym. Sci., Part B: Polym. Phys.* **2017**, *55*, 1075.
[53] R. Torres-Cavanillas, M. Gavara-Edo, E. Coronado, *Adv. Mater.* **2024**, *36*, 2307718.
[54] L. Torsi, M. Magliulo, K. Manoli, G. Palazzo, *Chem. Soc. Rev.* **2013**, *42*, 8612.
[55] A. Dodabalapur, L. Torsi, H. E. Katz, *Science* **1995**, *268*, 270.
[56] S. K. Park, Y. H. Kim, J. I. Han, D. G. Moon, W. K. Kim, M. G. Kwak, *Synth. Met.* **2003**, *139*, 377.
[57] H. Yang, T. J. Shin, L. Yang, K. Cho, C. Y. Ryu, Z. Bao, *Adv. Funct. Mater.* **2005**, *15*, 671.
[58] S. E. Alavi, B. Martin, Y. Zan, X. Yang, M. Piedrahita-Bello, W. Nicolazzi, J. F. Ganghoffer, L. Salmon, G. Molnar, A. Bousseksou, *Chem. Mater.* **2023**, *35*, 3276.
[59] C. Liao, M. Zhang, M. Y. Yao, T. Hua, L. Li, F. Yan, *Adv. Mater.* **2015**, *27*, 7493.
[60] Y. H. Lee, M. Jang, M. Y. Lee, O. Y. Kweon, J. H. Oh, *Chem* **2017**, *3*, 724.
[61] S. L. Ling, Z. Zheng, F. Yan, *Small Methods* **2018**, *2*, 1800070.
[62] C. Wang, H. Dong, L. Jiang, W. Hu, *Chem. Soc. Rev.* **2018**, *47*, 422.
[63] E. Orgiu, P. Samorì, *Adv. Mater.* **2014**, *26*, 1827.
[64] Y. Wakayama, R. Hayakawa, K. Higashiguchi, K. Matsuda, *J. Mater. Chem. C* **2020**, *8*, 10956.
[65] Y. Zan, L. Salmon, A. Bousseksou, *Nanomaterials* **2021**, *11*, 3169.